Environmental Science & Technology

Article

Cite This: Environ. Sci. Technol. 2019, 53, 12519−12528

pubs.acs.org/est

Relationships between Particulate Matter, Ozone, and Nitrogen Oxides during Urban Smoke Events in the Western US

Claire E. Buysse,*[,†] Aaron Kaulfus,[‡] Udaysankar Nair,[‡] and Daniel A. Jaffe*[,†,§]

[†]Department of Atmospheric Sciences, University of Washington, Seattle, Washington 98195, United States

[‡]Department of Atmospheric Science, University of Alabama in Huntsville, Huntsville, Alabama 35899, United States

[§]School of Science, Technology, Engineering, and Mathematics, University of Washington-Bothell, Bothell, Washington 98011, United States

Supporting Information

ABSTRACT: Urban ozone (O_3) pollution is influenced by the transport of wildfire smoke but observed impacts are highly variable. We investigate O_3 impacts from smoke in 18 western US cities during July−September, 2013−2017, with ground-based monitoring data from air quality system sites, using satellite-based hazard mapping system (HMS) fire and smoke product to identify overhead smoke. We present four key findings. First, O_3 and $PM_{2.5}$ (particulate matter <2.5 μm in diameter) are elevated at nearly all sites on days influenced by smoke, with the greatest mean enhancement occurring during multiday smoke events; nitrogen oxides (NO_x) are not consistently elevated across all sites. Second, $PM_{2.5}$ and O_3 exhibit a nonlinear relationship such that O_3 increases with $PM_{2.5}$ at low to moderate 24 h $PM_{2.5}$, peaks around 30−50 μg m^{-3}, and declines at higher $PM_{2.5}$. Third, the rate of increase of morning O_3 is higher and NO/NO_2 ratios are lower on smoke-influenced days, which could result from additional atmospheric oxidants in smoke. Fourth, while the HMS product is a useful tool for identifying smoke, O_3 and $PM_{2.5}$ are elevated on days before and after HMS-identified smoke events implying that a significant fraction of smoke events is not detected.

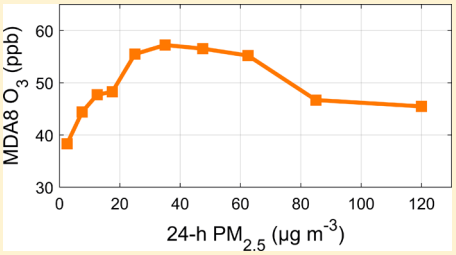

INTRODUCTION

Smoke from wildland fires is a persistent threat to air quality in the US. Both human- and natural-ignited fires burn throughout the western US during late summer, releasing large plumes of smoke into the atmosphere. With past[1,2] and projected[3−5] increases in western US fire activity, the degradation of air quality[6,7] and associated public health impacts[8,9] during smoke events are alarming. While surface-level particulate matter (PM) concentrations are visibly impacted during these events, impacts on ozone (O_3) are less clear.[10−12]

Wildland fires emit carbon monoxide (CO), PM, nitrogen oxides (NO_x = NO + NO_2), and a wide range of volatile organic compounds (VOCs). Because NO_x and VOCs are key O_3 precursors, their emission from fires is important to O_3 production. Fire NO_x emissions are a function of combustion efficiency, which can vary temporally within a single fire, and fuel nitrogen, which varies by tree species and biomass type.[13−15] VOC emissions are also complex and vary by fuel type,[16] though recent work suggests two temperature-dependent VOC emissions profiles similar across western US fuel types.[17] The high variability in direct emission of NO_x and VOCs from fires results in differing rates of near-source O_3 production. As smoke is transported away from the source, the photochemical environment changes, driving changes in O_3 mixing ratios. An important driver of these O_3 changes during transport is the lifetime and partitioning of reactive nitrogen species such as inorganic nitrate species, which serve as an atmospheric sink for NO_x, and peroxyacetyl nitrate (PAN), a chemical species associated with long-range O_x (O_x = O_3 + NO_2) storage.[18,19] Low-altitude transport of smoke may also drive the increased deposition of O_3 and O_3 precursors. The production of O_3 from wildland fires is further modulated by meteorological conditions associated with fire that affect O_3 photochemistry (e.g., temperature).[20,21]

With complex interactions between emissions, transport, and meteorology, it is challenging to predict downwind O_3 and large uncertainties remain.[22] This complexity is enhanced when smoke is transported into urban areas with large sources of NO_x, which have historically been targeted by emission controls to reduce the maximum daily 8 h average (MDA8) O_3. However, the nonlinearity of O_3 sensitivity to NO_x means that at high NO_x concentrations, additional NO_x facilitates O_3 destruction via NO titration while additional VOCs increase O_3 production. Since wildland fire emissions tend to be enriched in VOCs relative to NO_x,[16] the interception of smoke by a NO_x-rich urban area can lead to elevated O_3 levels.[23] This enhancement of urban O_3 production due to precursor transport supplements the direct transport of O_3 produced in the plume prior to interception. The combination of these O_3 impacts can exacerbate urban O_3 pollution and lead to exceedances of the O_3 national ambient air quality standard

Received: August 30, 2019
Revised: October 8, 2019
Accepted: October 10, 2019
Published: October 10, 2019

DOI: 10.1021/acs.est.9b05241
Environ. Sci. Technol. 2019, 53, 12519−12528

(NAAQS).[24] Because the design value for the O_3 NAAQS targets the most polluted days of the year, which typically occur in summer, the episodic addition of wildfire emissions in the same season can bring cities out of attainment. While cities may petition the Environmental Protection Agency (EPA) for exemption due to the occurrence of an exceptional event,[25] variability and an incomplete understanding of smoke impacts on O_3 make it difficult to verify. Further, public health impacts remain the same regardless of what data is excluded from regulatory consideration.

While smoke has the potential to significantly influence urban O_3 mixing ratios, actual impacts are difficult to determine and highly variable O_3 impacts have been observed.[10,23,26] Simulating these O_3 impacts with photochemical models has proven challenging for several reasons, including incomplete emissions data,[27] high sensitivity to meteorology,[28] and difficulty capturing heterogeneous chemistry.[29] Further, traditional grid models do not simulate smoke plume photochemistry well, especially as it relates to downwind O_3.[10,12,21,30−35] While Lagrangian parcel models have had some success,[36] more work is needed.

O_3 impacts may instead be assessed observationally using chemical tracers, and several tracers have been used as indicators of smoke, including CO,[37] acetonitrile,[13,38] water-soluble potassium (K^+),[39−41] levoglucosan,[42,43] and $PM_{2.5}$/CO ratios ($PM_{2.5}$ = particulate matter <2.5 μm in diameter).[44] However, fuel type and combustion temperature can modulate the emission of many chemical tracers from wildland fires,[45−47] complicating quantitative analyses of smoke influence. In addition, background concentrations of tracers may not be highly predictable in certain locations (e.g., CO in heavily polluted cities) and most smoke tracers are not routinely measured; $PM_{2.5}$ is often the only tracer available at regulatory air quality monitoring stations. In the absence of tracers, statistical modeling is useful for quantifying changes in O_3 during smoke events,[11,35,48] but this technique provides little insight into the mechanism of O_3 production.

The extended Leighton relationship is another approach to explore the drivers of O_3 production in smoke. This relationship represents the photochemical cycling of NO_x through O_3,[49,50] as well as HO_2 and RO_2

$$\frac{[NO]}{[NO_2]} = \frac{j(NO_2)}{k_{O_3}[O_3] + k_{HO_2}[HO_2] + k_{RO_2}[RO_2]}$$

where $j(NO_2)$ is the photolysis rate for the reaction

$$NO_2 + h\nu \rightarrow NO + O \quad (1)$$

k_{O_3} is the rate constant for the reaction

$$O_3 + NO \rightarrow NO_2 + O_2 \quad (2)$$

k_{HO_2} is the rate constant for the reaction

$$HO_2 + NO \rightarrow NO_2 + OH \quad (3)$$

and k_{RO_2} is the rate constant for the reaction

$$RO_2 + NO \rightarrow NO_2 + RO \quad (4)$$

A recent application of this relationship to two smoke plumes of moderate $PM_{2.5}$ (30−40 $\mu g\ m^{-3}$) found higher NO/NO_2 ratios with limited impacts on $j(NO_2)$ and O_3 production suggesting that RO_2 and HO_2 concentrations were lower in the plume than in adjacent air,[51] though this result does not align with anticipated VOC enhancements in smoke plumes.[16]

The present work has three aims. First, we quantify the impact of smoke in 18 western US cities on three urban pollutants: $PM_{2.5}$, O_3, and NO_x. Second, we investigate relationships between $PM_{2.5}$, NO_x, and O_3 during smoke events to identify patterns in the response of urban O_3. Third, we explore the photochemical controls over O_3 production during smoke events using the extended Leighton relationship and discuss current knowledge gaps.

DATA AND METHODS

We utilize the hazard mapping system fire and smoke product (hereafter abbreviated HMS),[52,53] provided by the National Oceanic and Atmospheric Administration's National Environmental Satellite, Data, and Information Service, as an indicator of smoke in the atmospheric column. HMS is a daily satellite-based product designed to identify fire hot spots and smoke plumes. While initial detections are automated, a human analyst verifies detections and outlines smoke plumes using infrared imagery to differentiate smoke from clouds. This technique may treat smoke plumes with high vapor content (e.g., pyrocumulus) as clouds, excluding them from identification as smoke. In addition, HMS will not identify smoke in the absence of an aerosol layer, though O_3 may still be impacted. The daily HMS product is typically created between 8:00 and 10:00 ET but is adjusted as additional satellite data becomes available, such that the daily product includes analysis of multiple satellite images. While these isolated snapshots are unable to perfectly capture smoke coverage, they are likely representative. In this work, individual HMS smoke plume polygons are merged to create a daily analysis of smoke areal extent, which is then used to generate a binary indicator of smoke at each site.[54]

Because HMS is a spatial product derived from top−down satellite imagery, its detection capability is limited by resolution (1 km) and cloud cover, among other factors, and it does not include vertical information about smoke coverage. This limited detection capability may prevent proper identification of smoke plumes, especially in the presence of clouds. Even when no clouds are present, small smoke plumes may not be automatically identified due to averaging with neighboring pixels.[53] Additionally, it is more difficult to detect smoke plumes at a high solar angle[55] and when intermixed with anthropogenic haze, which is when smoke influence is most relevant to urban O_3 pollution. The lack of vertical information provided by HMS makes it difficult to determine whether HMS-identified smoke is present in the boundary layer or free troposphere. This information is highly relevant to O_3 photochemistry, as smoke impacts vary with height: urban O_3 is primarily produced in the boundary layer where photochemistry is sensitive to precursor emissions, but smoke aloft may impact O_3 production by changing photolysis rates, temperature, and atmospheric stability. Still, HMS is a valuable tool for identifying smoke, especially since chemical tracers are not always available or colocated.

Motivated by the challenges associated with identifying smoke via HMS, we define four smoke classifications that facilitate greater statistical separation of smoke influence. First, days with no HMS-identified smoke are separated into two classes: those immediately preceding or following an HMS-identified smoke event (before or after smoke) and all other nonsmoke days (nonsmoke). The reason for this is two fold. Because the primary HMS analysis is performed in the early morning (between 5:00 and 8:00 local time, LT, in the western

DOI: 10.1021/acs.est.9b05241
Environ. Sci. Technol. 2019, 53, 12519−12528

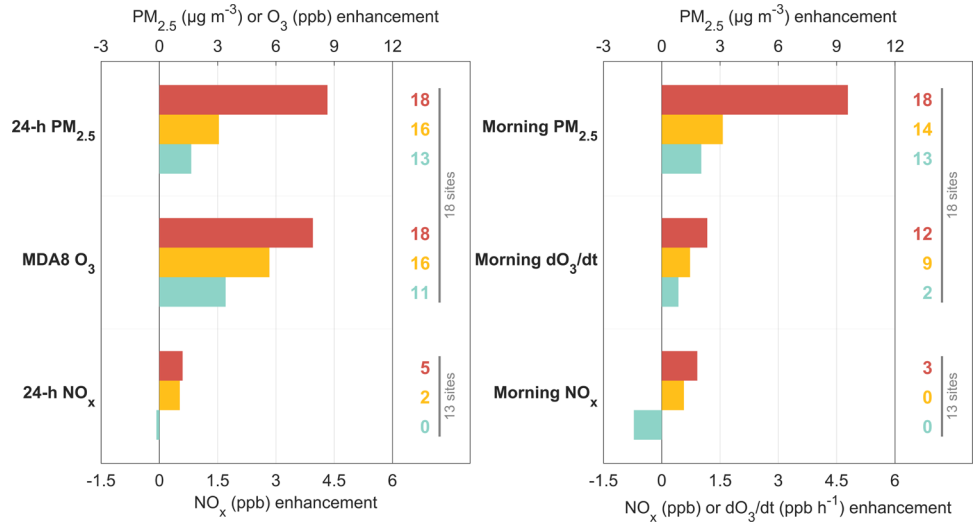

Figure 1. Mean enhancements relative to nonsmoke days for $PM_{2.5}$ (top), O_3 (center), and NO_x (bottom) for consecutive smoke (red), first smoke (gold), and before or after smoke (cyan) days. Data are displayed for daily (left) and morning (right) metrics. Numbers displayed to the right of each bar denote the number of sites with significant positive enhancements relative to nonsmoke days for each metric and smoke class.

US) each day, it is possible that days immediately preceding an HMS-identified smoke event may have daytime smoke that was not identified by HMS. In addition, days immediately before or after HMS-identified smoke events are more likely to have smoke because of their temporal proximity to other smoke events (e.g., winds favoring transport of smoke from a similar location) though smoke may not be identified in satellite imagery, as demonstrated by a case study presented in the Results and Discussion section. We recognize that this classification is not comprehensive and does not account for the misidentification of small smoke plumes or multiday pyrocumulus. In this work, the before or after smoke category is intended solely as an illustration of smoke impacts that are not captured by HMS. We employ the nonsmoke category as a nonfire seasonal mean for each site, assuming that nonfire sources of pollutants occur similarly in the presence and absence of smoke. This assumption may not hold if meteorology is strongly influenced by smoke (e.g., suppressed boundary layer mixing), which would increase nonfire pollutant concentrations during smoke events, or if thick smoke prevents some industrial activities, which would decrease smoke-influenced pollutant concentrations. Second, days with HMS-identified smoke are divided into two classes: the first day of an HMS-identified smoke event (first smoke) and any subsequent HMS-identified smoke days within a multiday smoke event (consecutive smoke). This separation serves to distinguish the compounded influence of smoke during multiday smoke events from the initial reception of smoke. Because sites may contribute a disproportionate number of days to each smoke class (i.e., sites with more smoke-influenced days may contribute fewer nonsmoke days), we calculate means for a given smoke class as an average of the individual site means.

We use hourly $PM_{2.5}$, O_3, nitric oxide (NO), nitrogen dioxide (NO_2), and temperature measurements, as well as 24 h $PM_{2.5}$ and MDA8 O_3 from air quality system (AQS) monitoring stations in 18 US cities from 2013 to 2017, downloaded via AirNow-Tech (www.airnowtech.org), a system operated for the US EPA. For four sites (Chico, Yuba City, Sacramento, and Denver), 24 h $PM_{2.5}$ data was unavailable at AirNow-Tech and was downloaded via the EPA's AQS Data Mart. Site-specific details about data collection are provided in Table S1, particularly when instrumentation does not follow federal reference or equivalent methods. Hourly measurements hosted by AirNow are compared against eight quality control criteria detailed in the Supporting Information with any measurements violating these criteria flagged for review by an AirNow operator. To minimize seasonal effects, only data from July to September are used. We exclude days without an available MDA8 O_3 or 24 h $PM_{2.5}$ value and at least 16 available hourly measurements for both $PM_{2.5}$ and O_3. When NO, NO_2, NO_x (NO + NO_2), or temperature data are presented, this availability criterion is additionally applied to hourly measurements. Missing hourly pollutant measurements that are isolated, having two available hourly measurements before and two after are replaced by the mean of the hour before and after. Negative hourly $PM_{2.5}$ measurements are removed if less than -5 $\mu g\ m^{-3}$, analogous to the default flag applied in AirNow data, or if they occur in an unclean atmosphere (following recommendation from the 2014 national ambient air monitoring conference),[56] which we define as $PM_{2.5}$ concentrations in the hour before and after being above 10 $\mu g\ m^{-3}$. We remove negative hourly O_3, NO, and NO_2 measurements and measurements greater than 3 standard deviations outside the 5 year hourly mean for O_3, NO, and NO_2 at each site. We exclude days that have hourly $PM_{2.5}$ concentrations more than 3 (nonsmoke) or 4 (all other classes) standard deviations outside the 24 h mean for a given day unless $PM_{2.5}$ variability is low (standard deviation $\leq$ 10 $\mu g\ m^{-3}$), considering the outlying data from these days to be nonreal or indicative of inconsistent and/or highly transient pollution events. Overall, these quality control measures have removed 6.9, 6.3, 7.6, and 6.5% of hourly O_3 and hourly $PM_{2.5}$, MDA8 O_3, and 24 h $PM_{2.5}$ data. For NO and NO_2 measurements, 19.4 and 19.2% have been removed primarily due to the required availability of all pollutants when data is used. For temperature measurements, <1% has been removed.

In this work, we utilize three daily metrics: 24 h $PM_{2.5}$, MDA8 O_3, and 24 h NO_x. We also compute three morning metrics that target peak O_3 production (morning $PM_{2.5}$, morning dO_3/dt, and morning NO_x) as well as morning NO/NO_2 ratios. Morning NO_x is computed as the hourly mean

DOI: 10.1021/acs.est.9b05241
Environ. Sci. Technol. 2019, 53, 12519−12528

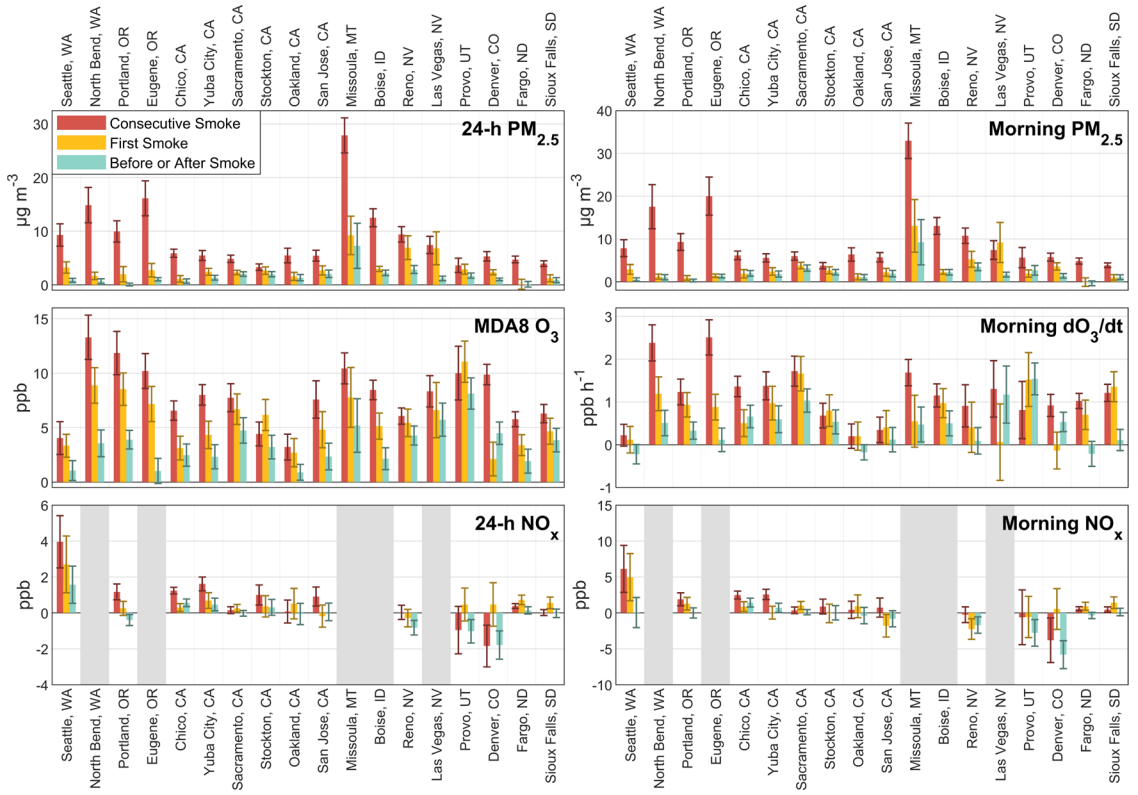

Figure 2. Mean enhancements relative to nonsmoke days by site for $PM_{2.5}$ (top), O_3 (center), and NO_x (bottom) for consecutive smoke (red), first smoke (gold), and before or after smoke (cyan) days. Data are displayed for daily (left) and morning (right) metrics. Error bars show standard error of the mean.

from 5:00 to 9:00 LT, when NO_x is typically at a maximum. Morning dO_3/dt is computed as the mean hourly increase in O_3 from 7:00 to 11:00 LT to capture subsequent peak O_3 production. Morning $PM_{2.5}$ and morning NO/NO_2 are computed as hourly means over the entire period from 5:00 to 11:00 LT. A Student's *t*-test is performed to determine statistical significance on before or after smoke, first smoke, and consecutive smoke days relative to nonsmoke days. Whenever mentioned in this work, significance is defined as $p < 0.05$.

RESULTS AND DISCUSSION

Identifying Smoke Influence. While we use HMS for smoke identification in this work, we acknowledge its limitations in resolution and cloud cover. To illustrate cloud interference in HMS smoke identification, we present a case study of HMS-identified smoke over Missoula, MT on August 28–30, 2015. Figure S1a–c shows moderate resolution imaging spectroradiometer visible imagery overlaid with the HMS fire and smoke product, in which overhead smoke was identified by HMS in Missoula on August 28th and 30th, but no smoke was identified by HMS on August 29th. However, surface monitors measured high concentrations of $PM_{2.5}$ during the 3 day period (Figure S1d), peaking at 183.6 $\mu g\ m^{-3}$ early on the morning of August 29th and remaining above 60 $\mu g\ m^{-3}$ throughout the day. In addition, 12 h back trajectories from Missoula at 500, 1000, and 1500 m at 12:00 LT on August 29th (Figure S2b) show air parcels that pass through several nearby fires just hours before arriving in Missoula, and high aerosol optical thickness immediately downwind of Missoula on the following day (Figure S2c) implies a large passage of smoke through the area. Collectively, this evidence strongly indicates that smoke was present in Missoula on August 29th, although it was not identified by HMS.

The misidentification of smoke days like the case presented here narrows the statistical difference between smoke and nonsmoke days. We attempt to account for some of this narrowing by defining four smoke classes, as described in the Data and Methods section: nonsmoke, before or after smoke, first smoke, and consecutive smoke.

Observed Pollution Enhancements. In Figure 1, we report the absolute mean enhancement of O_3, $PM_{2.5}$, and NO_x across all sites relative to the nonsmoke mean at each site. Because of high variability across sites, we report the number of sites with values in each smoke class that are significantly ($p < 0.05$) higher than values on nonsmoke days, rather than the collective standard error. Significantly lower values relative to nonsmoke days are only found at one site (Denver, CO) for one pollutant (NO_x), and this significance is not included in Figure 1. Mean enhancements and standard error by site are shown in Figure 2.

On average, $PM_{2.5}$ and O_3 are elevated relative to nonsmoke days in each smoke class and for both daily and morning metrics. The largest enhancements and the greatest number of sites with significant positive enhancements are found for consecutive smoke days, followed by first smoke and before or after smoke days, respectively. $PM_{2.5}$ (24 h and morning) is significantly enhanced at all sites on consecutive smoke days relative to nonsmoke days. For additional comparison, exceedances of the daily NAAQS (24 h $PM_{2.5} \geq 35.5\ \mu g\ m^{-3}$) occur on 7.3% of consecutive smoke days but <0.1% of

DOI: 10.1021/acs.est.9b05241
Environ. Sci. Technol. 2019, 53, 12519–12528

nonsmoke days, on average across all sites. MDA8 O_3 is also significantly enhanced at all sites on consecutive smoke days, and MDA8 O_3 exceedances (MDA8 O_3 > 70.9 ppb) occur on 4.6% of consecutive smoke days but <0.5% of nonsmoke days. Notably, 13 and 11 (of 18) sites also have significantly enhanced 24 h $PM_{2.5}$ and MDA8 O_3 on before or after smoke days, with exceedances occurring on 0.5 and 1.4% of before or after smoke days, respectively. This suggests a nontrivial influence of smoke on $PM_{2.5}$ and O_3 even though HMS does not detect smoke. We note that O_3 enhancements on smoke days may be partly attributable to temperature. This effect is most apparent in Fargo, ND, where smoke data is skewed toward higher temperatures (Figure S10). We control for this skew by computing the residual O_3 between HMS-identified smoke days and a linear fit of the nonsmoke data. We find that the median O_3 smoke residual is greater than 1 ppb at 13 of 16 sites and greater than 3 ppb at 9 of 16 sites, suggesting consistent positive O_3 enhancements from smoke at similar temperatures.

NO_x enhancements are relatively small for both daily and morning metrics, with the largest mean enhancement occurring in the morning on consecutive smoke days (0.9 ppb). NO_x enhancements are variable on before or after smoke days with less than 0.1 ppb change in mean NO_x for both metrics; a reduction in morning NO_x is statistically significant at one site (Denver, CO). On consecutive smoke days, significant positive enhancements in NO_x metrics are observed in Seattle, WA, Portland, OR (24 h only), Chico, CA, Yuba City, CA, and Fargo, ND (24 h only). The lack of a consistent trend in NO_x enhancements across sites and smoke classes implies high variability between smoke events and modest NO_x enhancements compared to urban variability. This is not unreasonable, given observed variability in NO_x in smoke plumes, which is often attributed to fuel nitrogen,[57,58] combustion efficiency,[59,60] and PAN chemistry.[18,28,61,62]

At individual sites, relative mean enhancements in 24 h $PM_{2.5}$ and morning $PM_{2.5}$ on consecutive smoke days range from 36 and 41% (Stockton, CA) to 535 and 558% (Missoula, MT), respectively. For MDA8 O_3 and morning dO_3/dt, enhancements range from 10% (Stockton, CA) and 8% (San Jose, CA) to 42% (North Bend, WA) and 63% (Eugene, OR), respectively. For 24 h NO_x and morning NO_x, enhancements range from −8% (Provo, UT) and −9% (Denver, CO) to 34 and 37% (Yuba City, CA), respectively. Percent enhancements are generally largest in the northwestern US (WA, OR, ID, MT), though Fargo, ND and Sioux Falls, SD see substantial relative enhancements in morning dO_3/dt (35 and 38% on consecutive smoke days, respectively). The high variability in $PM_{2.5}$ enhancements across sites may be partly attributable to the prevalence of nearby biomass burning events,[63] particularly in Boise, ID and Missoula, MT, as well as local circulation patterns. Differences in cloud cover and, thus, heterogeneous chemistry may also be linked to variability in $PM_{2.5}$ (see Tomaz et al.[64]) and water-soluble VOCs that affect O_3 production (e.g., de Gouw et al.[65] and references therein), though these effects may not be detected at the surface.

Relationship between $PM_{2.5}$ and O_3. In Figure 3, we demonstrate a nonlinear relationship between $PM_{2.5}$ and O_3, showing boxplots of site mean MDA8 O_3 for 10 $PM_{2.5}$ bins on all HMS-identified smoke days (first smoke and consecutive smoke days combined) and on nonsmoke days (excluding before or after smoke days). $PM_{2.5}$ bin sizes are increased at moderate and high $PM_{2.5}$ to maximize data availability and

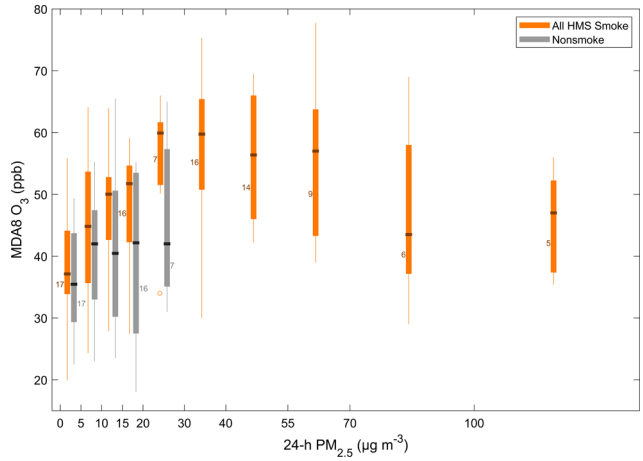

Figure 3. Boxplots of mean MDA8 O_3 at each site binned by 24 h $PM_{2.5}$ on all HMS-identified smoke (orange; first smoke and consecutive smoke) and nonsmoke (gray) days. If all sites (18) are not available for a given $PM_{2.5}$ bin, the number of contributing sites is displayed next to the boxplot. When both HMS-identified smoke and nonsmoke boxplots are shown for the same $PM_{2.5}$ bin, only sites that contribute to both categories are displayed. Boxplots with less than five contributing sites are not shown.

coverage across all sites. We use site means to equally weight nonsmoke and HMS-identified smoke contributions from each site. For the relationship between MDA8 O_3 and 24 h $PM_{2.5}$ at individual sites, see Figure S4. While the nonlinear dependence of O_3 on NO_x has been widely demonstrated (e.g., Pusede et al.[66]) to our knowledge, no such relationship has been identified for O_3 and $PM_{2.5}$. In part, this is because $PM_{2.5}$ has various indirect effects on O_3 production chemistry, and the relationship between these pollutants is not causal.

In general, we observe that MDA8 O_3 increases approximately linearly with 24 h $PM_{2.5}$ at low to moderate $PM_{2.5}$, up to ∼30 $\mu g\ m^{-3}$. Above this $PM_{2.5}$ concentration, MDA8 O_3 mixing ratios plateau and are more variable, with a range as large as 45 ppb. Median MDA8 O_3 noticeably declines above 24 h $PM_{2.5}$ concentrations of 70 $\mu g\ m^{-3}$. Collectively, this indicates a nonlinear relationship in which elevated $PM_{2.5}$ is associated with reduced O_3 mixing ratios, on average.

The observed decline in MDA8 O_3 at high 24 $PM_{2.5}$ may explain why mean enhancements in $PM_{2.5}$ on consecutive smoke days, which have the highest mean $PM_{2.5}$ concentrations, do not display similarly large enhancements in O_3. For some smoke events, O_3 suppression at high $PM_{2.5}$ could be attributable to concurrent NO_x enhancements due to NO_x titration of O_3. However, smoke-influenced NO_x enhancements can be marginal or absent, and observed enhancements in NO_x are likely to be accompanied by large VOC enhancements, which may shift NO_x-suppressed (NO-titrated) regimes toward NO_x sensitivity. This suggests that NO titration is unlikely to be the primary driver of the observed O_3 suppression, although it may be important in individual cases.[67]

Aside from changes in NO_x, several other effects associated with high $PM_{2.5}$ can impact O_3 mixing ratios. First, $PM_{2.5}$ concentrations in smoke may be associated with plume age and, as a result, O_3 production. High $PM_{2.5}$ concentrations are typically indicative of fresh plumes, which have produced less O_3 and, consequently, have lower O_3/CO ratios,[10] while lower $PM_{2.5}$ concentrations are associated with aged plumes, more

DOI: 10.1021/acs.est.9b05241
Environ. Sci. Technol. 2019, 53, 12519−12528

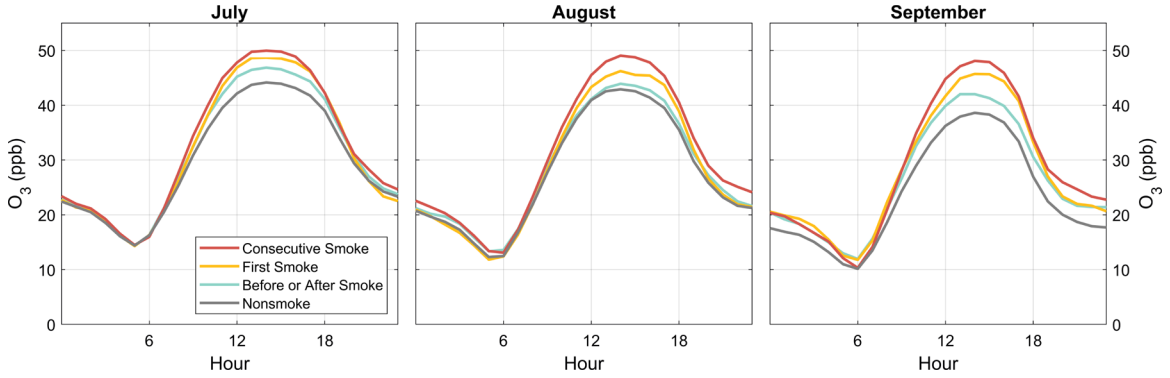

Figure 4. Eighteen-site mean diurnal O_3 profiles by month for consecutive smoke (red), first smoke (gold), before or after smoke (cyan), and nonsmoke (gray) days.

O_3 production, and higher O_3/CO ratios. However, the dilution of the plume may obscure this signal such that absolute O_3 mixing ratios are not correlated with O_3/CO ratios or plume age. Second, high $PM_{2.5}$ concentrations are likely to impact solar radiation, affecting O_3 production chemistry. Elevated $PM_{2.5}$ in urban areas may reduce direct solar radiation and, thus, the photolysis of NO_2, a key reaction in the production of O_3.[68,69] However, increases in aerosol scattering may offset some of this effect, with moderate enhancements in photolysis due to aerosol scattering observed at midday.[51,70,71] Reduced direct radiation can also reduce temperature, decreasing photochemical reaction rates important in O_3 production. Reductions in temperature and solar radiation, especially during smoke transport through forested regions, may also decrease the biogenic emission of isoprene,[72,73] an important contributor to organic reactivity and O_3 production.[74,75] In general, these combined effects are likely to reduce O_3 production. Third, $PM_{2.5}$ may affect the deposition of oxidants, including O_3 and O_3 precursors. Enhanced $PM_{2.5}$ can increase the total aerosol surface area and, as a result, the depositional sink of O_3. An increase in O_3 deposition may be paired with an increase in the deposition of NO_x, reactive VOCs, and/or HO_2 that contribute to O_3 formation, which would also reduce O_3 mixing ratios. Given the large variability in plume conditions, it is not clear which effect may dominate. Recent modeling work links increases in urban O_3 in China to a reduction in the aerosol sink of HO_2 radicals, suggesting that changes in the HO_2 sink may dominate in some environments.[76] Fourth, high $PM_{2.5}$ may suppress boundary layer mixing.[77] In the absence of smoke, this would promote the accumulation of O_3 precursors at the surface;[69] however, suppressed mixing in the presence of smoke aloft may also reduce the impact of smoke O_3 and O_3 precursors on mixing ratios at the surface. Fifth, $PM_{2.5}$ may alter cloud properties, indirectly affecting O_3 production chemistry. $PM_{2.5}$ has been observed to affect cloud formation[78−80] and cloud radiative properties,[81,82] which, in turn, may change photolysis rates and temperature. However, because of the uncertainty and variability in the role of smoke−cloud interactions, consistent impacts on temperature and photolysis are difficult to identify.

Our analysis indicates suppressed mean MDA8 O_3 at high 24 h $PM_{2.5}$ relative to moderate 24 h $PM_{2.5}$. Because the highest smoke $PM_{2.5}$ concentrations occur near the source, this finding is in line with observations that the largest O_3 impacts are typically some distance downwind of the source.[10,83] Additionally, at moderate $PM_{2.5}$, we find higher MDA8 O_3 on HMS-identified smoke days than on nonsmoke days at the same 24 $PM_{2.5}$ concentrations. This implies that reductions in direct solar radiation, which would suppress O_3 formation, are not a major driver of O_3 differences on smoke and nonsmoke days at low to moderate $PM_{2.5}$. Instead, elevated O_3 on smoke-influenced days is more likely to reflect the addition of VOCs into NO_x-suppressed (VOC-sensitive) urban areas or the addition of O_3 itself.

Diurnal Variability in O_3. To further explore what drives elevated MDA8 O_3 on smoke days, we examine diurnal O_3 profiles (Figures 4 and S6). Across all sites, O_3 generally increases more quickly in the morning when influenced by smoke, which is most apparent on consecutive smoke days, while morning minimum O_3 remains relatively constant across all four smoke classes. Differences in morning O_3 production across sites and smoke classes are quantified by the morning dO_3/dt metric (Figures 1 and 2). Observed enhancements in morning dO_3/dt are not a consequence of seasonality in the dataset as the same pattern emerges separately in July, August, and September (Figure 4).

These diurnal patterns suggest that additional O_3 is produced on smoke days, beginning in the morning, which argues against direct transport of O_3 into the boundary layer. Although morning O_3 production is larger on consecutive smoke days, it is responsible for a similar fraction (64%, nonsmoke; 65%, consecutive smoke) of total daily O_3 production. This implies that more rapid morning boundary layer growth cannot be solely responsible for differences in O_3. However, it is not obvious whether increased morning dO_3/dt is driven by enhanced photochemical production of O_3 or greater entrainment of O_3 stored in the residual layer. It is possible to explore these hypotheses by using the extended Leighton relationship to isolate variables of the photochemical environment that drive O_3 production in smoke plumes. Based on this relationship, the ratio of NO to NO_2 will be the same if there is no difference in the rate of photochemical reactions 1−4 or the concentration of photochemical species NO_2, O_3, HO_2, or RO_2. If O_3 photochemistry is substantially altered in smoke plumes, we suspect that NO/NO_2 ratios will also be different.

In Figure 5, we show morning NO/NO_2 ratios for each site and smoke class, since differences in diurnal O_3 variability are manifest in the morning. We exclude days with 24 h $PM_{2.5}$ greater than 30 $\mu g\ m^{-3}$ to minimize smoke impacts on $j(NO_2)$ and any differences in temperature resulting from changes in the absorption of solar radiation. Sites have an average of 146, 60, 36, and 59 days of data for nonsmoke, before or after smoke, first smoke, and consecutive smoke; Provo, UT, has the

DOI: 10.1021/acs.est.9b05241
Environ. Sci. Technol. 2019, 53, 12519−12528

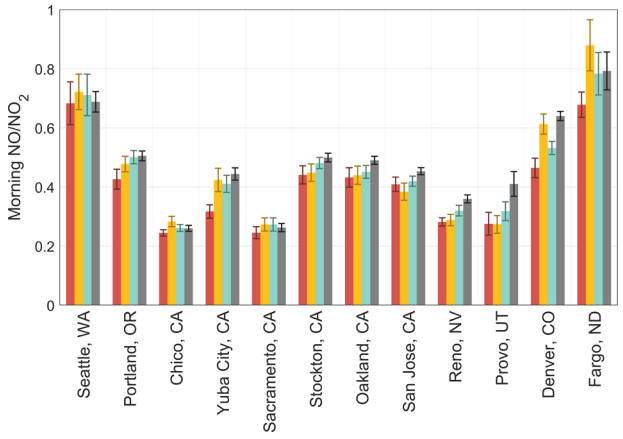

Figure 5. Mean morning (5:00−11:00 LT) NO/NO_2 ratios by site when 24 h $PM_{2.5}$ is less than or equal to 30 $\mu g\ m^{-3}$ for consecutive smoke (red), first smoke (gold), before or after smoke (cyan), and nonsmoke (gray) days. Error bars show standard error of the mean.

fewest days of data (44, 21, 12, and 12 for nonsmoke, before or after smoke, first smoke, and consecutive smoke) since the dataset spans only 2 years.

On average, NO/NO_2 ratios are lower at nearly all sites when influenced by smoke. Morning NO/NO_2 ratios on consecutive smoke days are significantly lower than on nonsmoke days at 5 (of 13) sites. In select cases, decreased NO/NO_2 ratios are also evident overnight (e.g., Fargo, ND), which is likely due to the carryover of high O_3 from the previous day (Figure S7). These lower NO/NO_2 ratios contrast Baylon et al.,[51] who observed higher NO/NO_2 ratios during two smoke events, though this earlier result was not explained by the authors. The lower NO/NO_2 ratios we observe on smoke-influenced days may arise for several reasons: (1) elevated atmospheric oxidants (O_3, HO_2, or RO_2), (2) higher temperatures driving a larger k_{O_3}, (3) lower rates of NO_2 photolysis, or (4) increased interference in NO_2 measurements by other reactive nitrogen species.

First, the transport of additional atmospheric oxidants in smoke would decrease NO/NO_2 ratios. Enhancements of oxidant species have been widely observed in smoke plumes (e.g., Liu et al.[84]). In many urban areas, NO_x-suppressed O_3 production chemistry would be sensitive to additional O_3, HO_2, and RO_2 species. As such, it is not unlikely that additional oxidant species are responsible for O_3 enhancements and/or faster photochemical production of O_3 in smoke.

Second, higher temperatures on smoke-influenced days may drive faster O_3 production and lower morning NO/NO_2 ratios. Statistically higher temperatures are observed on smoke-influenced days (Figure S8). At similar temperatures, morning dO_3/dt is not consistently higher or lower on smoke-influenced days (Figure S9), and it is possible that higher morning dO_3/dt and lower morning NO/NO_2 ratios may be partly driven by temperature differences. However, MDA8 O_3 is generally enhanced on smoke-influenced days at similar temperatures (Figures S9 and S10), suggesting that temperature effects are not the primary driver of high daytime O_3 during smoke events, particularly at high temperatures.

Third, it is possible that lower photolysis rates may occur on smoke-influenced days. However, only small changes have been observed[51] and lower photolysis rates would not explain observed increases in O_3. In the absence of photolysis measurements, we show NO/NO_2 ratios on days with low to moderate surface-level $PM_{2.5}$ to minimize radiative smoke effects, but we are unable to rule out changes in photolysis from smoke or clouds aloft.

Fourth, instrumental interference may result in inflated NO_2 measurements that contribute to lower NO/NO_2 ratios observed in smoke. Positive interference from reactive nitrogen species is widely recognized in chemiluminescence instruments that utilize a molybdenum NO_2 converter.[85] These instruments are employed at most sites in this work. While this interference is generally small for fresh NO_x-rich emissions that dominate the morning reactive nitrogen budget, the addition of reactive nitrogen from an aged smoke plume could increase positive instrumental interference and artificially inflate NO_2 measurements, resulting in lower NO/NO_2 ratios.

In sum, we identify large enhancements in $PM_{2.5}$ and O_3 on days with consecutive smoke influence as well as significant enhancements on days before and after HMS-identified smoke events. We present a nonlinear relationship between $PM_{2.5}$ and O_3, with reduced O_3 mixing ratios at high $PM_{2.5}$. This may occur for a variety of reasons including younger plume age, reduced solar radiation, and/or increased oxidant deposition to aerosol particles. With more comprehensive measurements (i.e., photolysis frequencies, VOCs, tracers of plume age) and photochemical modeling, the drivers of this nonlinear relationship could be better characterized. We also observe enhanced morning dO_3/dt and lower NO/NO_2 ratios in smoke, although the mechanism is unclear. Further research with reliable NO_x measurements alongside measurements of HO_2, RO_2, and photolysis rates could better constrain the contribution of atmospheric oxidants, particularly VOC reactivity, that may drive elevated O_3 during urban smoke events.

■ ASSOCIATED CONTENT

Supporting Information

The Supporting Information is available free of charge on the ACS Publications website at DOI: 10.1021/acs.est.9b05241.

Monitoring station data and instrumentation; case study of HMS smoke identification; mean nonsmoke pollutant levels; relationship between O_3/NO_x and $PM_{2.5}$; diurnal profiles of O_3 and NO/NO_2 ratios; temperature−O_3 comparisons (PDF)

■ AUTHOR INFORMATION

Corresponding Authors

*E-mail: cebuysse@uw.edu (C.E.B.).
*E-mail: djaffe@uw.edu (D.A.J.).

ORCID

Claire E. Buysse: 0000-0002-2324-1590
Daniel A. Jaffe: 0000-0003-1965-9051

Author Contributions

C.E.B. and D.A.J. conceived this study. A.K. and U.N. performed the HMS smoke product analysis. C.E.B. and D.A.J. were involved in air quality data analysis, scientific interpretation, and discussion. C.E.B. wrote the manuscript with contributions from all other co-authors.

Notes

The authors declare no competing financial interest.

DOI: 10.1021/acs.est.9b05241
Environ. Sci. Technol. 2019, 53, 12519−12528

■ ACKNOWLEDGMENTS

The work of C.E.B. and D.A.J. was supported by the National Science Foundation Grant 1447832 and National Oceanic and Atmospheric Administration Grant NA17OAR431001. Work of A.K. and U.N. was supported by National Science Foundation CAREER Grant AGS-1352046. We thank the US EPA for the use of publicly available AQS data collected from the EPA, state, local, and tribal monitoring agencies.

■ REFERENCES

(1) Westerling, A. L. Increasing western US forest wildfire activity: sensitivity to changes in the timing of spring. *Philos. Trans. R. Soc., B* **2016**, *371*, No. 20150178.

(2) Dennison, P. E.; Brewer, S. C.; Arnold, J. D.; Moritz, M. A. Large wildfire trends in the western United States, 1984−2011. *Geophys. Res. Lett.* **2014**, *41*, 2928−2933.

(3) Yue, X.; Mickley, L. J.; Logan, J. A.; Kaplan, J. O. Ensemble projections of wildfire activity and carbonaceous aerosol concentrations over the western United States in the mid-21st century. *Atmos. Environ.* **2013**, *77*, 767−780.

(4) Kitzberger, T.; Falk, D. A.; Westerling, A. L.; Swetnam, T. W. Direct and indirect climate controls predict heterogeneous early-mid 21st century wildfire burned area across western and boreal North America. *PLoS One* **2017**, *12*, No. e0188486.

(5) Stavros, E. N.; Abatzoglou, J. T.; McKenzie, D.; Larkin, N. K. Regional projections of the likelihood of very large wildland fires under a changing climate in the contiguous Western United States. *Clim. Change* **2014**, *126*, 455−468.

(6) McClure, C. D.; Jaffe, D. A. US particulate matter air quality improves except in wildfire-prone areas. *Proc. Natl. Acad. Sci. U.S.A.* **2018**, *115*, 7901−7906.

(7) Jaffe, D.; Hafner, W.; Chand, D.; Westerling, A.; Spracklen, D. Interannual Variations in PM2.5 due to Wildfires in the Western United States. *Environ. Sci. Technol.* **2008**, *42*, 2812−2818.

(8) Reid, C. E.; Brauer, M.; Johnston Fay, H.; Jerrett, M.; Balmes John, R.; Elliott Catherine, T. Critical review of health impacts of wildfire smoke exposure. *Environ. Health Perspect.* **2016**, *124*, 1334−1343.

(9) Cascio, W. E. Wildland fire smoke and human health. *Sci. Total Environ.* **2018**, *624*, 586−595.

(10) Jaffe, D. A.; Wigder, N. L. Ozone production from wildfires: A critical review. *Atmos. Environ.* **2012**, *51*, 1−10.

(11) Gong, X.; Kaulfus, A.; Nair, U.; Jaffe, D. A. Quantifying O_3 Impacts in Urban Areas Due to Wildfires Using a Generalized Additive Model. *Environ. Sci. Technol.* **2017**, *51*, 13216−13223.

(12) Baker, K. R.; Woody, M. C.; Tonnesen, G. S.; Hutzell, W.; Pye, H. O. T.; Beaver, M. R.; Pouliot, G.; Pierce, T. Contribution of regional-scale fire events to ozone and PM2.5 air quality estimated by photochemical modeling approaches. *Atmos. Environ.* **2016**, *140*, 539−554.

(13) Andreae, M. O.; Merlet, P. Emission of trace gases and aerosols from biomass burning. *Global Biogeochem. Cycles* **2001**, *15*, 955−966.

(14) Burling, I. R.; Yokelson, R. J.; Griffith, D. W. T.; Johnson, T. J.; Veres, P.; Roberts, J. M.; Warneke, C.; Urbanski, S. P.; Reardon, J.; Weise, D. R.; Hao, W. M.; de Gouw, J. Laboratory measurements of trace gas emissions from biomass burning of fuel types from the southeastern and southwestern United States. *Atmos. Chem. Phys.* **2010**, *10*, 11115−11130.

(15) Andreae, M. O. Emission of trace gases and aerosols from biomass burning − an updated assessment. *Atmos. Chem. Phys.* **2019**, *19*, 8523−8546.

(16) Akagi, S. K.; Yokelson, R. J.; Wiedinmyer, C.; Alvarado, M. J.; Reid, J. S.; Karl, T.; Crounse, J. D.; Wennberg, P. O. Emission factors for open and domestic biomass burning for use in atmospheric models. *Atmos. Chem. Phys.* **2011**, *11*, 4039−4072.

(17) Sekimoto, K.; Koss, A. R.; Gilman, J. B.; Selimovic, V.; Coggon, M. M.; Zarzana, K. J.; Yuan, B.; Lerner, B. M.; Brown, S. S.; Warneke, C.; Yokelson, R. J.; Roberts, J. M.; de Gouw, J. High- and low-temperature pyrolysis profiles describe volatile organic compound emissions from western US wildfire fuels. *Atmos. Chem. Phys.* **2018**, *18*, 9263−9281.

(18) Alvarado, M. J.; Logan, J. A.; Mao, J.; Apel, E.; Riemer, D.; Blake, D.; Cohen, R. C.; Min, K. E.; Perring, A. E.; Browne, E. C.; Wooldridge, P. J.; Diskin, G. S.; Sachse, G. W.; Fuelberg, H.; Sessions, W. R.; Harrigan, D. L.; Huey, G.; Liao, J.; Case-Hanks, A.; Jimenez, J. L.; Cubison, M. J.; Vay, S. A.; Weinheimer, A. J.; Knapp, D. J.; Montzka, D. D.; Flocke, F. M.; Pollack, I. B.; Wennberg, P. O.; Kurten, A.; Crounse, J.; Clair, J. M. S.; Wisthaler, A.; Mikoviny, T.; Yantosca, R. M.; Carouge, C. C.; Le Sager, P. Nitrogen oxides and PAN in plumes from boreal fires during ARCTAS-B and their impact on ozone: an integrated analysis of aircraft and satellite observations. *Atmos. Chem. Phys.* **2010**, *10*, 9739−9760.

(19) Fischer, E. V.; Jacob, D. J.; Yantosca, R. M.; Sulprizio, M. P.; Millet, D. B.; Mao, J.; Paulot, F.; Singh, H. B.; Roiger, A.; Ries, L.; Talbot, R. W.; Dzepina, K.; Pandey Deolal, S. Atmospheric peroxyacetyl nitrate (PAN): a global budget and source attribution. *Atmos. Chem. Phys.* **2014**, *14*, 2679−2698.

(20) Lin, M.; Horowitz, L. W.; Payton, R.; Fiore, A. M.; Tonnesen, G. US surface ozone trends and extremes from 1980 to 2014: quantifying the roles of rising Asian emissions, domestic controls, wildfires, and climate. *Atmos. Chem. Phys.* **2017**, *17*, 2943−2970.

(21) Zhang, L.; Jacob, D. J.; Yue, X.; Downey, N. V.; Wood, D. A.; Blewitt, D. Sources contributing to background surface ozone in the US Intermountain West. *Atmos. Chem. Phys.* **2014**, *14*, 5295−5309.

(22) Jaffe, D. A.; Cooper, O. R.; Fiore, A. M.; Henderson, B. H.; Tonnesen, G. S.; Russell, A. G.; Henze, D. K.; Langford, A. O.; Lin, M. Y.; Moore, T. Scientific assessment of background ozone over the US: Implications for air quality management. *Elementa* **2018**, *6*, No. 56.

(23) Singh, H. B.; Cai, C.; Kaduwela, A.; Weinheimer, A.; Wisthaler, A. Interactions of fire emissions and urban pollution over California: Ozone formation and air quality simulations. *Atmos. Environ.* **2012**, *56*, 45−51.

(24) Environmental Protection Agency (EPA). National Ambient Air Quality Standards for Ozone. *Fed. Regist.* **2015**, *80*, 65291−65468.

(25) Environmental Protection Agency. *Guidance on the Preparation of Exceptional Events Demonstrations for Wildfire Events that May Influence Ozone Concentrations*; US EPA: Research Triangle Park, NC, 2016.

(26) Jaffe, D.; Chand, D.; Hafner, W.; Westerling, A.; Spracklen, D. Influence of Fires on O_3 Concentrations in the Western U.S. *Environ. Sci. Technol.* **2008**, *42*, 5885−5891.

(27) Lawson, S. J.; Cope, M.; Lee, S.; Galbally, I. E.; Ristovski, Z.; Keywood, M. D. Biomass burning at Cape Grim: exploring photochemistry using multi-scale modelling. *Atmos. Chem. Phys.* **2017**, *17*, 11707−11726.

(28) Mason, S. A.; Trentmann, J.; Winterrath, T.; Yokelson, R. J.; Christian, T. J.; Carlson, L. J.; Warner, T. R.; Wolfe, L. C.; Andreae, M. O. Intercomparison of two box models of the chemical evolution in biomass-burning smoke plumes. *J. Atmos. Chem.* **2006**, *55*, 273−297.

(29) Jacob, D. J. Heterogeneous chemistry and tropospheric ozone. *Atmos. Environ.* **2000**, *34*, 2131−2159.

(30) Alvarado, M. J.; Wang, C.; Prinn, R. G. Formation of ozone and growth of aerosols in young smoke plumes from biomass burning: 2. Three-dimensional Eulerian studies. *J. Geophys. Res.: Atmos.* **2009**, *114*, No. D09307.

(31) Zhang, L.; Jacob, D. J.; Downey, N. V.; Wood, D. A.; Blewitt, D.; Carouge, C. C.; van Donkelaar, A.; Jones, D. B. A.; Murray, L. T.; Wang, Y. Improved estimate of the policy-relevant background ozone in the United States using the GEOS-Chem global model with 1/2° × 2/3° horizontal resolution over North America. *Atmos. Environ.* **2011**, *45*, 6769−6776.

(32) Lu, X.; Zhang, L.; Yue, X.; Zhang, J.; Jaffe, D. A.; Stohl, A.; Zhao, Y.; Shao, J. Wildfire influences on the variability and trend of summer surface ozone in the mountainous western United States. *Atmos. Chem. Phys.* **2016**, *16*, 14687−14702.

DOI: 10.1021/acs.est.9b05241
Environ. Sci. Technol. 2019, 53, 12519−12528

(33) Emery, C.; Jung, J.; Downey, N.; Johnson, J.; Jimenez, M.; Yarwood, G.; Morris, R. Regional and global modeling estimates of policy relevant background ozone over the United States. *Atmos. Environ.* **2012**, *47*, 206−217.
(34) Baker, K. R.; Woody, M. C.; Valin, L.; Szykman, J.; Yates, E. L.; Iraci, L. T.; Choi, H. D.; Soja, A. J.; Koplitz, S. N.; Zhou, L.; Campuzano-Jost, P.; Jimenez, J. L.; Hair, J. W. Photochemical model evaluation of 2013 California wild fire air quality impacts using surface, aircraft, and satellite data. *Sci. Total Environ.* **2018**, *637-638*, 1137−1149.
(35) Jaffe, D. A.; Wigder, N.; Downey, N.; Pfister, G.; Boynard, A.; Reid, S. B. Impact of Wildfires on Ozone Exceptional Events in the Western U.S. *Environ. Sci. Technol.* **2013**, *47*, 11065−11072.
(36) Alvarado, M. J.; Prinn, R. G. Formation of ozone and growth of aerosols in young smoke plumes from biomass burning: 1. Lagrangian parcel studies. *J. Geophys. Res.: Atmos.* **2009**, *114*, No. D09306.
(37) Briggs, N. L.; Jaffe, D. A.; Gao, H. L.; Hee, J. R.; Baylon, P. M.; Zhang, Q.; Zhou, S.; Collier, S. C.; Sampson, P. D.; Cary, R. A. Particulate Matter, Ozone, and Nitrogen Species in Aged Wildfire Plumes Observed at the Mount Bachelor Observatory. *Aerosol Air Qual. Res.* **2016**, *16*, 3075−3087.
(38) de Gouw, J. A.; Warneke, C.; Parrish, D. D.; Holloway, J. S.; Trainer, M.; Fehsenfeld, F. C. Emission sources and ocean uptake of acetonitrile (CH_3CN) in the atmosphere. *J. Geophys. Res.: Atmos.* **2003**, *108*, No. 4329.
(39) Ramadan, Z.; Song, X. H.; Hopke, P. K. Identification of sources of Phoenix aerosol by positive matrix factorization. *J. Air Waste Manag. Assoc.* **2000**, *50*, 1308−1320.
(40) Nie, W.; Ding, A. J.; Xie, Y. N.; Xu, Z.; Mao, H.; Kerminen, V. M.; Zheng, L. F.; Qi, X. M.; Huang, X.; Yang, X. Q.; Sun, J. N.; Herrmann, E.; Petäjä, T.; Kulmala, M.; Fu, C. B. Influence of biomass burning plumes on HONO chemistry in eastern China. *Atmos. Chem. Phys.* **2015**, *15*, 1147−1159.
(41) Popovicheva, O. B.; Engling, G.; Diapouli, E.; Saraga, D.; Persiantseva, N. M.; Timofeev, M. A.; Kireeva, E. D.; Shonija, N. K.; Chen, S.-H.; Nguyen, D. L.; Eleftheriadis, K.; Lee, C.-T. Impact of Smoke Intensity on Size-Resolved Aerosol Composition and Microstructure during the Biomass Burning Season in Northwest Vietnam. *Aerosol Air Qual. Res.* **2016**, *16*, 2635−2654.
(42) Popovicheva, O. B.; Kozlov, V. S.; Rakhimov, R. F.; Shmargunov, V. P.; Kireeva, E. D.; Persiantseva, N. M.; Timofeev, M. A.; Engling, G.; Eleftheriadis, K.; Diapouli, E.; Panchenko, M. V.; Zimmermann, R.; Schnelle-Kreis, J. Optical-microphysical and physical-chemical characteristics of Siberian biomass burning: Experiments in Aerosol Chamber. *Atmos. Oceanic Opt.* **2016**, *29*, 492−500.
(43) Khamkaew, C.; Chantara, S.; Janta, R.; Pani, S. K.; Prapamontol, T.; Kawichai, S.; Wiriya, W.; Lin, N.-H. Investigation of Biomass Burning Chemical Components over Northern Southeast Asia during 7-SEAS/BASELInE 2014 Campaign. *Aerosol Air Qual. Res.* **2016**, *16*, 2655−2670.
(44) Laing, J. R.; Jaffe, D. A.; Slavens, A. P.; Li, W.; Wang, W. Can ΔPM2.5/ΔCO and ΔNOy/ΔCO Enhancement Ratios Be Used to Characterize the Influence of Wildfire Smoke in Urban Areas? *Aerosol Air Qual. Res.* **2017**, *17*, 2413−2423.
(45) Echalar, F.; Gaudichet, A.; Cachier, H.; Artaxo, P. Aerosol emissions by tropical forest and savanna biomass burning: Characteristic trace elements and fluxes. *Geophys. Res. Lett.* **1995**, *22*, 3039−3042.
(46) Lee, T.; Sullivan, A. P.; Mack, L.; Jimenez, J. L.; Kreidenweis, S. M.; Onasch, T. B.; Worsnop, D. R.; Malm, W.; Wold, C. E.; Hao, W. M.; Collett, J. L. Chemical Smoke Marker Emissions During Flaming and Smoldering Phases of Laboratory Open Burning of Wildland Fuels. *Aerosol Sci. Technol.* **2010**, *44*, I−V.
(47) Shafizadeh, F. Introduction to pyrolysis of biomass. *J. Anal. Appl. Pyrolysis* **1982**, *3*, 283−305.
(48) McClure, C. D.; Jaffe, D. A. Investigation of high ozone events due to wildfire smoke in an urban area. *Atmos. Environ.* **2018**, *194*, 146−157.
(49) Leighton, P. A. *Photochemistry of Air Pollution*; Academic Press: New York, 1961; Vol. *9*.
(50) Finlayson-Pitts, B. J.; Pitts, J. N., Jr. *Chemistry of the Upper and Lower Atmosphere*; Academic Press: San Diego, 2000.
(51) Baylon, P.; Jaffe, D. A.; Hall, S. R.; Ullmann, K.; Alvarado, M. J.; Lefer, B. L. Impact of Biomass Burning Plumes on Photolysis Rates and Ozone Formation at the Mount Bachelor Observatory. *J. Geophys. Res.: Atmos.* **2018**, *123*, 2272−2284.
(52) Rolph, G. D.; Draxler, R. R.; Stein, A. F.; Taylor, A.; Ruminski, M. G.; Kondragunta, S.; Zeng, J.; Huang, H.-C.; Manikin, G.; McQueen, J. T.; Davidson, P. M. Description and Verification of the NOAA Smoke Forecasting System: The 2007 Fire Season. *Weather Forecast.* **2009**, *24*, 361−378.
(53) Ruminski, M.; Kondragunta, S.; Draxler, R.; Zeng, J. In *Recent Changes to the Hazard Mapping System*, Proceedings of the 15th International Emissions Inventory Conference, New Orleans, LA, 2006.
(54) Kaulfus, A. S.; Nair, U.; Jaffe, D.; Christopher, S. A.; Goodrick, S. Biomass Burning Smoke Climatology of the United States: Implications for Particulate Matter Air Quality. *Environ. Sci. Technol.* **2017**, *51*, 11731−11741.
(55) McNamara, D.; Stephens, G.; Ruminski, M.; Kasheta, T. *The Hazard Mapping System (HMS) - NOAA'S Multi-Sensor Fire and Smoke Detection Program Using Environmental Satellites*, 2004.
(56) Hanley, T.; Weinstock, L. In *PM Continuous Training*, Proceedings of the National Ambient Air Monitoring Conference, Environmental Protection Agency: Portland, OR, 2018.
(57) Lacaux, J. P.; Delmas, R.; Jambert, C.; Kuhlbusch, T. A. J. NOx emissions from African savanna fires. *J. Geophys. Res.: Atmos* **1996**, *101*, 23585−23595.
(58) Yokelson, R. J.; Urbanski, S. P.; Atlas, E. L.; Toohey, D. W.; Alvarado, E. C.; Crounse, J. D.; Wennberg, P. O.; Fisher, M. E.; Wold, C. E.; Campos, T. L.; Adachi, K.; Buseck, P. R.; Hao, W. M. Emissions from forest fires near Mexico City. *Atmos. Chem. Phys.* **2007**, *7*, 5569−5584.
(59) Hiroshi, T.; Kohei, I.; Boersma, K. F.; Ronald, J. vdA.; Savitri, G. Interannual variability of nitrogen oxides emissions from boreal fires in Siberia and Alaska during 1996−2011 as observed from space. *Environ. Res. Lett.* **2015**, *10*, No. 065004.
(60) McMeeking, G. R.; Kreidenweis, S. M.; Baker, S.; Carrico, C. M.; Chow, J. C.; Collett, J. L.; Hao, W. M.; Holden, A. S.; Kirchstetter, T. W.; Malm, W. C.; Moosmüller, H.; Sullivan, A. P.; Wold, C. E. Emissions of trace gases and aerosols during the open combustion of biomass in the laboratory. *J. Geophys. Res.: Atmos.* **2009**, *114*, No. D19210.
(61) Mauzerall, D. L.; Logan, J. A.; Jacob, D. J.; Anderson, B. E.; Blake, D. R.; Bradshaw, J. D.; Heikes, B.; Sachse, G. W.; Singh, H.; Talbot, B. Photochemistry in biomass burning plumes and implications for tropospheric ozone over the tropical South Atlantic. *J. Geophys. Res.: Atmos.* **1998**, *103*, 8401−8423.
(62) Val Martín, M.; Honrath, R. E.; Owen, R. C.; Pfister, G.; Fialho, P.; Barata, F. Significant enhancements of nitrogen oxides, black carbon, and ozone in the North Atlantic lower free troposphere resulting from North American boreal wildfires. *J. Geophys. Res.: Atmos.* **2006**, *111*, No. 1.
(63) Brey, S. J.; Ruminski, M.; Atwood, S. A.; Fischer, E. V. Connecting smoke plumes to sources using Hazard Mapping System (HMS) smoke and fire location data over North America. *Atmos. Chem. Phys.* **2018**, *18*, 1745−1761.
(64) Tomaz, S.; Cui, T.; Chen, Y.; Sexton, K. G.; Roberts, J. M.; Warneke, C.; Yokelson, R. J.; Surratt, J. D.; Turpin, B. J. Photochemical Cloud Processing of Primary Wildfire Emissions as a Potential Source of Secondary Organic Aerosol. *Environ. Sci. Technol.* **2018**, *52*, 11027−11037.
(65) de Gouw, J. A.; Warneke, C.; Stohl, A.; Wollny, A. G.; Brock, C. A.; Cooper, O. R.; Holloway, J. S.; Trainer, M.; Fehsenfeld, F. C.; Atlas, E. L.; Donnelly, S. G.; Stroud, V.; Lueb, A. Volatile organic compounds composition of merged and aged forest fire plumes from

DOI: 10.1021/acs.est.9b05241
Environ. Sci. Technol. 2019, 53, 12519−12528

Alaska and western Canada. *J. Geophys. Res.: Atmos.* **2006**, *111*, No. D10303.
(66) Pusede, S. E.; Cohen, R. C. On the observed response of ozone to NOx and VOC reactivity reductions in San Joaquin Valley California 1995-present. *Atmos. Chem. Phys.* **2012**, *12*, 8323−8339.
(67) Baylon, P.; Jaffe, D. A.; Wigder, N. L.; Gao, H.; Hee, J. Ozone enhancement in western US wildfire plumes at the Mt. Bachelor Observatory: The role of NOx. *Atmos. Environ.* **2015**, *109*, 297−304.
(68) Bian, H.; Han, S.; Tie, X.; Sun, M.; Liu, A. Evidence of impact of aerosols on surface ozone concentration in Tianjin, China. *Atmos. Environ.* **2007**, *41*, 4672−4681.
(69) Xing, J.; Wang, J.; Mathur, R.; Wang, S.; Sarwar, G.; Pleim, J.; Hogrefe, C.; Zhang, Y.; Jiang, J.; Wong, D. C.; Hao, J. Impacts of aerosol direct effects on tropospheric ozone through changes in atmospheric dynamics and photolysis rates. *Atmos. Chem. Phys.* **2017**, *17*, 9869−9883.
(70) Dickerson, R. R.; Kondragunta, S.; Stenchikov, G.; Civerolo, K. L.; Doddridge, B. G.; Holben, B. N. The Impact of Aerosols on Solar Ultraviolet Radiation and Photochemical Smog. *Science* **1997**, *278*, 827−830.
(71) Li, G.; Bei, N.; Tie, X.; Molina, L. T. Aerosol effects on the photochemistry in Mexico City during MCMA-2006/MILAGRO campaign. *Atmos. Chem. Phys.* **2011**, *11*, 5169−5182.
(72) Geron, C.; Guenther, A.; Sharkey, T.; Arnts, R. R. Temporal variability in basal isoprene emission factor. *Tree Physiol.* **2000**, *20*, 799−805.
(73) Xiaoshan, Z.; Yujing, M.; Wenzhi, S.; Yahui, Z. Seasonal variations of isoprene emissions from deciduous trees. *Atmos. Environ.* **2000**, *34*, 3027−3032.
(74) Williams, J.; Roberts, J. M.; Fehsenfeld, F. C.; Bertman, S. B.; Buhr, M. P.; Goldan, P. D.; Hübler, G.; Kuster, W. C.; Ryerson, T. B.; Trainer, M.; Young, V. Regional ozone from biogenic hydrocarbons deduced from airborne measurements of PAN, PPN, and MPAN. *Geophys. Res. Lett.* **1997**, *24*, 1099−1102.
(75) Trainer, M.; Williams, E. J.; Parrish, D. D.; Buhr, M. P.; Allwine, E. J.; Westberg, H. H.; Fehsenfeld, F. C.; Liu, S. C. Models and observations of the impact of natural hydrocarbons on rural ozone. *Nature* **1987**, *329*, 705−707.
(76) Li, K.; Jacob, D. J.; Liao, H.; Shen, L.; Zhang, Q.; Bates, K. H. Anthropogenic drivers of 2013−2017 trends in summer surface ozone in China. *Proc. Natl. Acad. Sci. U.S.A.* **2019**, *116*, 422.
(77) Wilcox, E. M.; Thomas, R. M.; Praveen, P. S.; Pistone, K.; Bender, F. A. M.; Ramanathan, V. Black carbon solar absorption suppresses turbulence in the atmospheric boundary layer. *Proc. Natl. Acad. Sci. U.S.A.* **2016**, *113*, 11794−11799.
(78) Feingold, G.; Jiang, H.; Harrington, J. Y. On smoke suppression of clouds in Amazonia. *Geophys. Res. Lett.* **2005**, *32*, No. L02804.
(79) Koren, I.; Kaufman, Y. J.; Remer, L. A.; Martins, J. V. Measurement of the Effect of Amazon Smoke on Inhibition of Cloud Formation. *Science* **2004**, *303*, 1342−1345.
(80) Koren, I.; Martins, J. V.; Remer, L. A.; Afargan, H. Smoke Invigoration Versus Inhibition of Clouds over the Amazon. *Science* **2008**, *321*, 946−949.
(81) Zamora, L. M.; Kahn, R. A.; Cubison, M. J.; Diskin, G. S.; Jimenez, J. L.; Kondo, Y.; McFarquhar, G. M.; Nenes, A.; Thornhill, K. L.; Wisthaler, A.; Zelenyuk, A.; Ziemba, L. D. Aircraft-measured indirect cloud effects from biomass burning smoke in the Arctic and subarctic. *Atmos. Chem. Phys.* **2016**, *16*, 715−738.
(82) Lu, Z.; Liu, X.; Zhang, Z.; Zhao, C.; Meyer, K.; Rajapakshe, C.; Wu, C.; Yang, Z.; Penner, J. E. Biomass smoke from southern Africa can significantly enhance the brightness of stratocumulus over the southeastern Atlantic Ocean. *Proc. Natl. Acad. Sci. U.S.A.* **2018**, *115*, 2924−2929.
(83) Brey, S. J.; Fischer, E. V. Smoke in the City: How Often and Where Does Smoke Impact Summertime Ozone in the United States? *Environ. Sci. Technol.* **2016**, *50*, 1288−1294.
(84) Liu, X.; Huey, L. G.; Yokelson, R. J.; Selimovic, V.; Simpson, I. J.; Müller, M.; Jimenez, J. L.; Campuzano-Jost, P.; Beyersdorf, A. J.; Blake, D. R.; Butterfield, Z.; Choi, Y.; Crounse, J. D.; Day, D. A.; Diskin, G. S.; Dubey, M. K.; Fortner, E.; Hanisco, T. F.; Hu, W.; King, L. E.; Kleinman, L.; Meinardi, S.; Mikoviny, T.; Onasch, T. B.; Palm, B. B.; Peischl, J.; Pollack, I. B.; Ryerson, T. B.; Sachse, G. W.; Sedlacek, A. J.; Shilling, J. E.; Springston, S.; St. Clair, J. M.; Tanner, D. J.; Teng, A. P.; Wennberg, P. O.; Wisthaler, A.; Wolfe, G. M. Airborne measurements of western U.S. wildfire emissions: Comparison with prescribed burning and air quality implications. *J. Geophys. Res.: Atmos.* **2017**, *122*, 6108−6129.
(85) Villena, G.; Bejan, I.; Kurtenbach, R.; Wiesen, P.; Kleffmann, J. Interferences of commercial NO_2 instruments in the urban atmosphere and in a smog chamber. *Atmos. Meas. Tech.* **2012**, *5*, 149−159.

DOI: 10.1021/acs.est.9b05241
Environ. Sci. Technol. 2019, 53, 12519−12528